Structural constraints limit the regime of optimal flux in autocatalytic reaction networks

Check for updates

Armand Despons [1] ✉, Yannick De Decker[2] & David Lacoste[1]

Autocatalytic chemical networks play a predominant role in a large number of natural systems such as in metabolic pathways and in ecological networks. Despite recent efforts, the precise impact of thermodynamic constraints on these networks remains elusive. In this work, we present a theoretical framework that allows specific bounds on the thermodynamic affinity and on the concentrations of autocatalysts in mass-action autocatalytic networks. These bounds can be obtained solely from the stoichiometry of the underlying chemical reaction network, and are independent from the numerical values of kinetic parameters. This property holds in the specific regime where all the fluxes of the network are tightly coupled and maximal. Our method is applicable to large networks, and can be used to complement constraints-based modeling methods of metabolic networks, which typically do not provide predictions about thermodynamic properties or concentration ranges of metabolites.

The dynamical properties of most systems found in nature can be traced back to a combination of chemical reactions that are maintained out of equilibrium. This is particularly the case in biology and ecology, where these chemical reaction networks can reach high levels of complexity. Many such networks involve autocatalysis, which is the ability of chemicals to catalyze their own formation[1,2]. Autocatalysis enables exponential growth[3,4], self-replication[5], and metabolism[6].

The properties of chemical reaction networks are constrained by non-equilibrium thermodynamics. For example, living systems are thought to self-organize thanks to energy and matter flows, which allow them to lower their own entropy at the expense of an entropy increase in the environment[7], as required by the second law. Thermodynamics is also believed to play a key role in chemical evolution[8,9] and in the organization of ecological communities[10,11]. Yet, understanding precisely the role played by thermodynamic constraints proved difficult both for biology and ecology, despite the many recent efforts on this issue[12–16]. Because of this, we still do not fully understand the fundamental principles by which chemical evolution operates, which limits our ability to design new materials with life-like properties.

This lack of general understanding also has more practical consequences. The knowledge we have about metabolic networks is rather limited as far as kinetics is concerned. For this reason, current modeling approaches for metabolic networks focus on predicting steady fluxes by optimizing an objective function with linear constraints, as in flux balance analysis[17,18] or in structural kinetic modeling[19]. These methods are general, valid for any chemical network and do not require a detailed knowledge of

the kinetics, but it is not easy to use them to make predictions about metabolite concentrations. For instance, at the moment, concentration ranges of metabolites can be predicted from these methods but only for mass-action networks[20].

The aforementioned problems are all related to the fact that while non-equilibrium thermodynamics is a well-established discipline, its implications for autocatalytic networks have not been fully explored yet. In this context, we develop a theoretical framework for autocatalytic chemical networks operating in a stationary non-equilibrium regime. This approach builds on a recent stoichiometric classification of autocatalytic chemical networks[21,22], which can be used to identify such networks thanks to chemoinformatic techniques[23–25]. We find that in a specific regime where fluxes in the network are tightly coupled and optimal, there is a connection between the topology of a network, the stoichiometry of its autocatalytic reactions, and the thermodynamic force keeping this network out of equilibrium. In this regime, we show that the force required to operate an autocatalytic network at a maximum rate obeys universal constraints, which depend on topology and stoichiometry, but are independent from the kinetic rate constants of the reactions. Because these constraints contain information on the topology of the network, they can be used to rule out certain network architectures for a given global autocatalytic reaction, even in the absence of any knowledge about kinetics. In the end, our work shows how thermodynamics constrains the chemical space accessible to autocatalysis, which is relevant for chemical evolution and Origin of Life studies. It also provides relevant information regarding the thermodynamics of autocatalytic
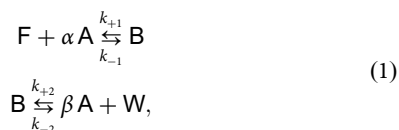
[1]Gulliver Laboratory, UMR CNRS 7083, PSL Research University, ESPCI, Paris F-75231, France. [2]Center for Nonlinear Phenomena and Complex Systems (CENOLI), Université libre de Bruxelles (ULB), Campus Plaine, C.P. 231, B-1050 Brussels, Belgium. ✉e-mail: armand.despons@espci.fr

networks and the concentration ranges of the autocatalysts, which could be useful in designing new chemical networks.

Results

Motivating example

Our objective is to find a connection between the rate of production of an autocatalytic process, its distance from equilibrium, and the stoichiometry of the underlying reaction network. Consider, for illustration, the following reactive system:

$$
\begin{aligned}
\mathsf{F} + \alpha\,\mathsf{A} &\underset{k_{-1}}{\overset{k_{+1}}{\rightleftharpoons}} \mathsf{B} \\
\mathsf{B} &\underset{k_{-2}}{\overset{k_{+2}}{\rightleftharpoons}} \beta\,\mathsf{A} + \mathsf{W},
\end{aligned}
\tag{1}
$$

with $\beta > \alpha > 0$. The topology of (1) is encoded in its stoichiometric matrix,

$$
\nabla = \begin{array}{c}
\mathsf{F} \\
\mathsf{W} \\
\mathsf{A} \\
\mathsf{B}
\end{array}
\begin{pmatrix}
-1 & 0 \\
0 & 1 \\
-\alpha & \beta \\
1 & -1
\end{pmatrix}.
\tag{2}
$$

The species F and W act as fuel and waste for the overall production of the other species. In what follows, we will treat their concentrations, f and w, as constants. Only a submatrix of (2) is required to capture the autocatalytic behavior of (1):

$$
\mathbb{S} = \begin{array}{c}
\mathsf{A} \\
\mathsf{B}
\end{array}
\begin{pmatrix}
-\alpha & \beta \\
1 & -1
\end{pmatrix}.
\tag{3}
$$

This submatrix establishes a connection between the time derivative of the concentrations of the autocatalytic species a and b with the reaction fluxes,

$$
d_t \begin{pmatrix} a \\ b \end{pmatrix} = \mathbb{S} \cdot \mathbf{j},
\tag{4}
$$

where $\mathbf{j}$ is a vector containing the fluxes of reactions 1 and 2, $\mathbf{j} = (j_1, j_2)^\top$. For ideal isothermal solutions, each of these reaction fluxes can be decomposed as the difference of two one-way fluxes obeying the law of mass action:

$$
j_{+1} = k_{+1} f\, a^\alpha, \qquad j_{-1} = k_{-1} b,
\tag{5}
$$

$$
j_{+2} = k_{+2} b, \qquad j_{-2} = k_{-2} a^\beta w;
\tag{6}
$$

and the components of $\mathbf{j}$ are $j_i = j_{+i} - j_{-i}$. Nothing prevents this reactive system from reaching the equilibrium state, since the concentrations of both A and B are unconstrained. To drive the network (1) away from its equilibrium state, we introduce a control mechanism which maintains the concentrations a or b constant thanks to an outgoing flux.

When the concentration of species A is controlled (chemostatted), the dynamics of the system is entirely controlled by the evolution law for b, $d_t b = j_1 - j_2$. The steady state is such that $j_1 = j_2$, which shows that there is a tight coupling[26] between the two reactions. Here, j_1 and j_2 are also equal to the production rate $\mathcal{J}$ of the overall reaction:

$$
\mathsf{F} + \alpha\,\mathsf{A} \longrightarrow \beta\,\mathsf{A} + \mathsf{W}.
\tag{7}
$$
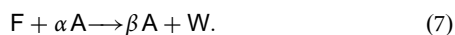
This reaction has an overall affinity (which is equal to the opposite of the Gibbs free energy ΔG) $\mathcal{A} = \mu_\mathsf{F} - \mu_\mathsf{W} - (\beta - \alpha)\mu_\mathsf{A}$, where μ_i is the

chemical potential of species i. Since μ_F and μ_W are fixed, fixing μ_A is essential to maintain the system in a non-equilibrium state where $\mathcal{A}$ is non-zero. Otherwise, the system will reach equilibrium, where the affinity vanishes. Solving for the steady-state concentration provides the expression for the macroscopic flux of production of species A:

$$
\mathcal{J} = \frac{k_{+1} k_{+2}}{k_{-1} + k_{+2}} \left[a^\alpha f - \left(\frac{k_{-1} k_{-2}}{k_{+1} k_{+2}} \right) a^\beta w \right].
\tag{8}
$$

Introducing the reaction quotient $Q = a^{(\beta - \alpha)} w / f$ and the equilibrium constant $K = k_{+1} k_{+2} / k_{-1} k_{-2}$ of the global reaction (7), it is easy to show that the global flux $\mathcal{J}$ has the same sign as the affinity, since $\mathcal{A} = \ln(K/Q)$ (we work with units where $RT = 1$). Furthermore, the current goes through a maximum as a function of a whenever

$$
\frac{a^{(\beta - \alpha)} w}{f} = \frac{\alpha}{\beta} \frac{k_{+1} k_{+2}}{k_{-1} k_{-2}},
\tag{9}
$$

which corresponds to the condition $Q = Q^* = \alpha/\beta \times K$. Thus, the maximum rate is reached when the chemical affinity becomes

$$
\mathcal{A}^* = \ln \frac{\beta}{\alpha}.
\tag{10}
$$

Hence, the distance from equilibrium at which the autocatalytic network achieves its optimal production rate, namely $\mathcal{A}^*$, is not fixed by the values of kinetic constants or by the equilibrium constant of the global process. It only depends on the stoichiometry of the overall reaction. We illustrate these results in Fig. 1, for the case $\alpha = 1$, $\beta = 2$. Note that this condition on the affinity can also be expressed in terms of the concentration a. Since $\exp(\mathcal{A}^*) = K/Q^*$, the point of maximum flux is given by

$$
\left(\frac{a^*}{a_{eq}} \right)^{\beta - \alpha} = \frac{\alpha}{\beta},
\tag{11}
$$

which means that optimality is reached when the concentration of the chemostat is at half its equilibrium value.

We can carry a similar analysis if, instead of A, B is the chemostatted autocatalytic species. Now, the dynamics is ruled by $d_t a = \beta j_2 - \alpha j_1$, and the steady state is such that $j_1/\beta = j_2/\alpha = \mathcal{J}$, which is the overall production rate of species B,

$$
\beta\,\mathsf{F} + \alpha\,\mathsf{B} \longrightarrow \beta\,\mathsf{B} + \alpha\,\mathsf{W}.
\tag{12}
$$

The steady-state solution now involves polynomials of different order, making it impossible to find explicitly the conditions maximizing the rate of production with the previous method. Nonetheless, we can determine $\mathcal{A}^*$ by numerically finding the value of Q^* that maximizes the global reaction rate for randomly generated values of the various kinetic constants. We find that the optimal affinity is now bounded from below (see Supplementary Note 12):

$$
\mathcal{A}^* \geq \ln \frac{\beta}{\alpha}.
\tag{13}
$$

Here too, the constraint acting on the optimal distance from equilibrium solely depends on the stoichiometry of the overall reaction. This thermodynamic constraint translates into a threshold for the value of the concentration of the controlled species, b^* as

$$
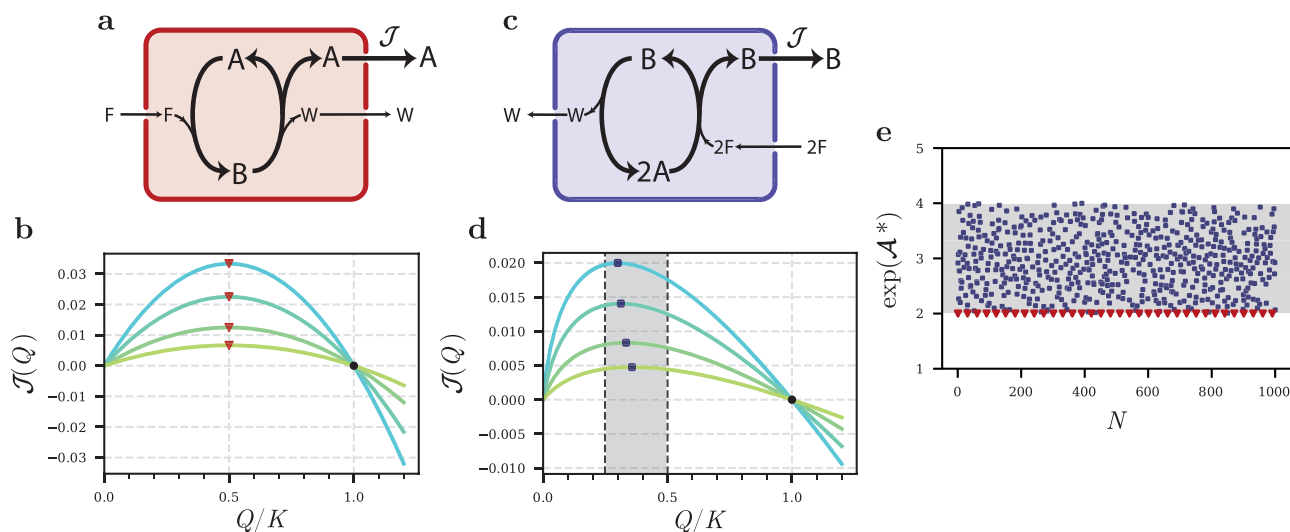\left(\frac{b^*}{b_{eq}} \right)^{\beta - \alpha} \leq \frac{\alpha}{\beta},
\tag{14}
$$

Fig. 1 | Selected properties of the autocatalytic system (1) for $\alpha = 1$ and $\beta = 2$.
a Representation of a reactor in which the concentrations of F, W, and A are maintained constant thanks to exchanges with external reservoirs (chemostats).
b The corresponding global flux $\mathcal{J}$ as a function of Q vanishes when $Q = K$ (on the black circle) and reaches a maximum at the same location $Q^* = K/2$ (red triangles).
c Species F, W are still chemostatted, but now B is chemostatted instead of A. **d** Now the maxima of the corresponding global reaction rate are reached at different

locations such that $1/4 \leq Q^*/K \leq 1/2$ (shaded gray area). Note that all the fluxes still vanish when $Q = K$. **e** Cloud of points for the exponential of the global affinity $\mathcal{A}^*$, for randomly chosen sets of kinetic rate constants indexed by N. When species A is controlled (red triangles), the optimal affinity always equals $\ln 2$, as explained in the main text. When species B is controlled (blue squares), the optimal affinity admits both a lower and upper bound, which corresponds to the gray area in the lower plot of **b**.

where b_{eq} is the equilibrium concentration of B. Note the importance of the condition $\beta > \alpha > 0$, which guarantees the invertibility of the stoichiometric matrix $\mathbb{S}$ and leads to equalities or inequalities Eqs. (10–14).

Figure 1 summarizes the behavior of the network Eq. (1) in the particular case $\alpha = 1$ and $\beta = 2$. It also reveals that, on top of the upper bound Eq. (14), the location of the global flux is also lower-bounded, $Q^*/K \geq 1/4$, yielding an upper bound for the affinity $\mathcal{A}^*$. This behavior can be recovered analytically for arbitrary values of α and β (see Supplementary Notes 11, 12).

General approach for autocatalytic chemical reaction networks (CRNs)

In what follows, we present a general approach that enables the computation of the overall affinity $\mathcal{A}^*$ corresponding to a condition of the local extremum of the global production rate. Our method relies on the stoichiometry of the reaction network, and circumvents the need to explicitly evaluate the steady states or reaction rates of the system under consideration.

Following a recent stoichiometric characterization of autocatalysis[21], a general autocatalytic network should contain one or several autocatalytic cores. An essential feature of these cores is that they are described by an invertible stoichiometric submatrix. The existence of this invertible submatrix is a sufficient condition for autocatalysis, which implies the absence of mass-like conservation laws[13,27,28] thanks to Gordan's theorem[21]. In the following, we assume that the full stoichiometric matrix ∇ contains a square submatrix $\mathbb{S}$ that is invertible:

$$\nabla = \begin{pmatrix} \nabla^{ex} \\ \cdots\cdots\cdots \\ \mathbb{S} \quad \vdots \quad 0 \end{pmatrix} \qquad (15)$$

Reactions of $\mathbb{S}$ will be called autocatalytic reactions, species of $\mathbb{S}$ will be called autocatalytic species, while other species will be called external. Note that we do not require that the matrix $\mathbb{S}$ corresponds necessarily to one of the autocatalytic cores listed in Table 1 of the Methods Section. Further, we also allow the network to contain catalytic reactions, (i.e., reactions where

the same species can be both reactants and products) in contrast with the assumptions of ref. 21. The presence of a block matrix of zero in the lower right part of the matrix ∇ in Eq. (15) means that there is no boundary flux to or from external species. Such a splitting of species into internal and external ones is a standard assumption in metabolic network analysis[29].

Similar to the example above, the concentrations of all external species are assumed to be constant, either because these species are in excess, which is typically the case for food or fuel species, or because they are in contact with a reservoir (chemostatted). Given the structure of the full stoichiometric matrix of Eq. (37), one can show that the network can satisfy detailed balance (see Eq. (38) and Supplementary Note 1). To break detailed balance, in addition, the concentration of at least one of the autocatalytic species should be controlled, by actively maintaining its concentration constant with an outgoing flux.

We call this special species the X species, and we call the remaining non-controlled autocatalytic ones the Y species. The stoichiometric matrix $\mathbb{S}$ splits into a row vector $\mathbf{S}^X$ and a matrix $\mathbb{S}^{Y}$[27]:

$$\mathbb{S} = \begin{pmatrix} \mathbf{S}^X \\ \mathbb{S}^Y \end{pmatrix}. \qquad (16)$$

The corresponding kinetic equations are given by

$$d_t x = \mathbf{S}^X \cdot \mathbf{j} + I = 0 \qquad (17)$$

$$d_t \mathbf{y} = \mathbb{S}^Y \cdot \mathbf{j}, \qquad (18)$$

where x denotes the concentration of species X and $\mathbf{y}$ is the concentration vector of all the Y species. The vector $\mathbf{j}$ contains the rates of the autocatalytic reactions, and I is a scalar function describing the exchange of matter with the chemostat.

The inverse $\mathbb{S}^{-1}$ plays an important role:

$$\mathbb{S}^{-1} = \{\mathbf{g}_\sigma\}_{Z_\sigma \in \mathcal{Z}}, \qquad (19)$$

where $\mathbf{g}_\sigma$ is the column of $\mathbb{S}^{-1}$ associated to species Z_σ, which denotes autocatalytic species of the X or of the Y type, and $\mathcal{Z}$ is the set of all the

Table 1 | Bounds on the chemical affinities at the maximum of the macroscopic flux for the five autocatalytic cores[21]

Motif	$\mathbb{S}$	$\mathbb{S}^{-1}$	Overall equation along g_X	Bound on $\mathcal{A}^*$
Type I	$\begin{array}{c}A\\B\\{}\end{array}\begin{pmatrix}-1 & 2\\1 & -1\\1 & 2\end{pmatrix}$	$\begin{array}{c}1\\2\\{}\end{array}\begin{pmatrix}1 & 2\\1 & 1\\A & B\end{pmatrix}$	$A + B \xrightarrow{g_A} 2A + B$ $2A + B \xrightarrow{g_B} 2A + 2B$	$\mathcal{A}^* = \ln 2$ $\mathcal{A}^* \geq \ln 2$
Type II	$\begin{array}{c}A\\B\\C\\{}\end{array}\begin{pmatrix}-1 & 0 & 1\\1 & -1 & 1\\0 & 1 & -1\\1 & 2 & 3\end{pmatrix}$	$\begin{array}{c}1\\2\\3\\{}\end{array}\begin{pmatrix}0 & 1 & 1\\1 & 1 & 2\\1 & 1 & 1\\A & B & C\end{pmatrix}$	$B + C \xrightarrow{g_A} A + B + C$ $A + B + C \xrightarrow{g_B} A + 2B + C$ $A + 2B + C \xrightarrow{g_C} A + 2B + 2C$	$\mathcal{A}^* = \ln 2$ $\mathcal{A}^* \geq \ln 2$ $\mathcal{A}^* \geq \ln 2$
Type III	$\begin{array}{c}A\\B\\C\\{}\end{array}\begin{pmatrix}-1 & 0 & 1\\1 & -1 & 1\\0 & 1 & -1\\1 & 2 & 3\end{pmatrix}$	$\begin{array}{c}1\\2\\3\\{}\end{array}\begin{pmatrix}1 & 1 & 1\\1 & 0 & 1\\1 & 1 & 0\\A & B & C\end{pmatrix}$	$A + B + C \xrightarrow{g_A} 2A + B + C$ $A + C \xrightarrow{g_B} A + B + C$ $A + B \xrightarrow{g_C} A + B + C$	$\mathcal{A}^* \geq \ln 2$ $\mathcal{A}^* \geq \ln 2$ $\mathcal{A}^* \geq \ln 2$
Type IV	$\begin{array}{c}A\\B\\C\\{}\end{array}\begin{pmatrix}-1 & 1 & 0\\1 & -1 & 1\\1 & 1 & -1\\1 & 2 & 3\end{pmatrix}$	$\begin{array}{c}1\\2\\3\\{}\end{array}\begin{pmatrix}0 & 1/2 & 1/2\\1 & 1/2 & 1/2\\1 & 1 & 0\\A & B & C\end{pmatrix}$	$B + C \xrightarrow{g_A} A + B + C$ $\frac{1}{2}A + \frac{1}{2}B + C \xrightarrow{g_B} \frac{1}{2}A + \frac{3}{2}B + C$ $\frac{1}{2}A + \frac{1}{2}B \xrightarrow{g_C} \frac{1}{2}A + \frac{1}{2}B + C$	$\mathcal{A}^* \geq \ln 3$ $\mathcal{A}^* \geq \frac{\ln 3}{2}$ $\mathcal{A}^* \geq \frac{\ln 3}{2}$
Type V	$\begin{array}{c}A\\B\\C\\{}\end{array}\begin{pmatrix}-1 & 1 & 1\\1 & -1 & 1\\1 & 1 & -1\\1 & 2 & 3\end{pmatrix}$	$\begin{array}{c}1\\2\\3\\{}\end{array}\begin{pmatrix}0 & 1/2 & 1/2\\1/2 & 0 & 1/2\\1/2 & 1/2 & 0\\A & B & C\end{pmatrix}$	$\frac{1}{2}B + \frac{1}{2}C \xrightarrow{g_A} A + \frac{1}{2}B + \frac{1}{2}C$ $\frac{1}{2}A + \frac{1}{2}C \xrightarrow{g_B} \frac{1}{2}A + B + \frac{1}{2}C$ $\frac{1}{2}A + \frac{1}{2}B \xrightarrow{g_C} \frac{1}{2}A + \frac{1}{2}B + C$	$\mathcal{A}^* \geq \ln 3$ $\mathcal{A}^* \geq \ln 3$ $\mathcal{A}^* \geq \ln 3$

autocatalytic species. It follows from the property of the inverse that $\mathbf{g}_\sigma$ represents a reaction pathway that produces a single unit of species Z_σ without affecting the other species (see Supplementary Note 2). For this reason, $\mathbf{g}_\sigma$ is the elementary mode of production of species Z_σ[21]. From all the elementary modes of production, one can build a reaction vector $\mathbf{g} = \sum_\sigma \mathbf{g}_\sigma$, which represents a combination of elementary modes that increases the amount of all the autocatalytic species by one unit:

$$\mathbb{S} \cdot \mathbf{g} = \mathbf{1}, \tag{20}$$

where $\mathbf{1}$ is a column vector full of ones. The existence of this vector is a sufficient condition for autocatalysis.

The steady-state of Eq. (18) is a vector belonging to the right nullspace of $\mathbb{S}^Y$[27,28], which is spanned by $\mathbf{g}_X$, the elementary mode of production associated with species X. Thus, the stationary flux vector can be written as

$$\mathbf{j} = \mathcal{J} \mathbf{g}_X, \tag{21}$$

which we call a tight coupling condition, since all elementary fluxes are proportional to the global production rate $\mathcal{J}$ with constant coefficients of proportionality. Since in general, $\mathbf{g}_X$ has rational components, it is convenient to rescale this vector to facilitate its interpretation as a mode of production. We show in the Methods section that, after the rescaling, the bounds on the global affinity are also rescaled by the same amount.

We now introduce assumptions about the dynamics of the network at the level of elementary reactions. Every such reaction denoted ρ is assumed to be reversible, with a net flux given by

$$j_\rho = j_{+\rho} - j_{-\rho}. \tag{22}$$

Here, one-way fluxes $j_{\pm\rho}$ obey mass-action kinetics[30,31]:

$$j_{\pm\rho} = k_{\pm\rho} \prod_\sigma z_\sigma^{S_{\pm\rho}^\sigma}, \tag{23}$$

where z_σ is the concentration of species Z_σ, and $\mathbb{S}_+$ (resp. $\mathbb{S}_-$) is the stoichiometric matrix associated to forward (resp. reverse) reactions, such that $\mathbb{S} = \mathbb{S}_- - \mathbb{S}_+$. Note that the constant concentrations of the fuel/food species have been absorbed in the effective rate constants $k_{\pm\rho}$. We choose to work with ideal solutions for clarity of presentation, but we show in Supplementary Note 4 that the results presented below remain valid for non-ideal solutions.

Overall affinity

The affinity of an elementary reaction is connected to fluxes by means of the flux–force relationship: $\mathcal{A}_\rho = \ln(j_{+\rho}/j_{-\rho})$. Taking the linear combination of the elementary affinities, we obtain the global affinity

$$\mathcal{A} = \sum_\rho g_X^\rho \mathcal{A}_\rho = \sum_\rho g_X^\rho \ln\left(\frac{j_{+\rho}}{j_{-\rho}}\right) = \ln\left(\frac{K}{Q}\right), \tag{24}$$

where K and Q are, respectively, the equilibrium constant and the reaction quotient Q[32]. Here, the reaction quotient coincides with the concentration of the controlled autocatalytic species ($Q = x$) because the concentrations of food species have been incorporated in the rate constants, and the stationary global flux is a function of this quantity, $\mathcal{J} = \mathcal{J}(Q)$.

We expect that in the cases of interest, this flux will present at least one maximum when the CRN is brought out of equilibrium. Indeed, due to the tight coupling condition, the total entropy production rate (EPR) in the steady-state has a simple expression[13,27,28]:

$$\Sigma = \sum_\rho j_\rho \mathcal{A}_\rho = \mathcal{J} \mathcal{A}. \tag{25}$$

The second law of thermodynamics dictates that $\Sigma \geq 0$, and equality is achieved at equilibrium, where $Q = K$ and both $\mathcal{J}$ and $\mathcal{A}$ vanish. It follows, from Eq. (24), that $\mathcal{J}(Q) \geq 0$ when $Q \in [0, K]$. Let us consider a class of autocatalytic networks, for which species X has a nucleating role[24]. In that case, the flux $\mathcal{J}(0)$ is zero when this species is absent (in other words, for $Q = 0$). This was the case, for example, with the simple autocatalytic system discussed earlier (see Fig. 1). For these networks, there must be at least one local extremum of the global flux in the interval $Q \in [0, K]$. This regime is optimal, in the sense that species X is produced at a maximal rate. Importantly, the extremum of the global flux and that of the EPR do not coincide because $\mathcal{A}$ in Eq. (24) is a non-linear function of Q which also enters in Eq. (25). This is in agreement with the observation that the optimal regime of operation of non-equilibrium systems generally does not correspond to a point where the EPR is extremum[33].

Response coefficients at maximum flux

We call Q^* the value of Q which makes the global flux maximal, with a zero derivative: $d_Q \mathcal{J} = 0$. Due to the tight coupling condition Eq. (21), all reaction fluxes are also at an extremum at Q^*: $d_Q j_\rho = d_Q j_{+\rho} - d_Q j_{-\rho} = 0$, for any reaction ρ. To characterize this configuration, we introduce the log-
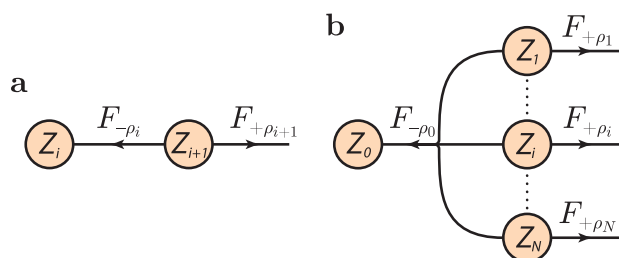
Fig. 2 | Structural constraints acting on the log-derivatives of the steady uni-directional fluxes with mass-action kinetics. a When a species Z_{i+1} is connected by unimolecular pathways upstream and downstream, the two outgoing one-way fluxes have equal log-derivative, $F_{-\rho_i} = F_{+\rho_{i+1}}$. **b** In a branched pathway, a species Z_0 is connected to various species Z_i, and the sum of the log-derivative of the forward flux of all products balances the log-derivative of the reverse branched reaction, $F_{-\rho_0} = \sum_i S^i_{-\rho_0} F_{+\rho_i}$.

derivative of the stationary elementary fluxes, which we call $F_{\pm\rho}$:

$$F_{\pm\rho} = d_Q \ln j_{\pm\rho} = \sum_\sigma S^\sigma_{\pm\rho} d_Q \ln z_\sigma. \tag{26}$$

These are the response coefficients of the steady unidirectional fluxes with respect to a change in Q. Because the $F_{\pm\rho}$s are log-derivatives, all the factors entering rate laws that do not depend on Q will not contribute to these coefficients. This includes the rate constants, which do not appear explicitly. Crucially, the coefficients $F_{\pm\rho}$s satisfy structural constraints related to the topology of the network. A graphical illustration of these structural relations is provided in Fig. 2 for the particular case of a linear and a branched reaction pathway. In the linear pathway, an arbitrary species Z_i is transformed into a product species Z_{i+1} by a reversible and unimolecular reaction ρ_i, and then Z_{i+1} undergoes a similar reaction ρ_{i+1}. In such case, both $j_{-\rho_i}$ and $j_{+\rho_{i+1}}$ depend solely on the concentration z_{i+1} of species Z_{i+1}. Consequently, $F_{-\rho_i} = F_{+\rho_{i+1}}$, because both terms are equal to $d_Q \ln z_{i+1}$. For the branched pathway, a species Z_0 splits through the reaction $+\rho_0$ into several products Z_i with multiplicity $S^i_{-\rho_0}$, and Eq. (26) leads to $F_{-\rho_0} = \sum_i S^i_{-\rho_0} F_{+\rho_i}$.

For a general network, these structural relations take a form analogous to Kirchoff's laws (see Supplementary Note 3):

$$\mathbf{F}_- = \mathbf{F}_+ \cdot \left(\mathbb{S}_+^{-1} \cdot \mathbb{S}_- \right), \tag{27}$$

provided $\mathbb{S}_+$ is invertible, which is the case in most networks of interest. Note that the definition of the coefficients $F_{\pm\rho}$ and the structural constraints Eq. (27) are valid even when $Q \neq Q^*$. The structural constraints acting on the $F_{\pm\rho}$s play a key role in our framework, because these coefficients are intimately related to the affinities at the optimal current. Indeed, when $Q = Q^*$ one has:

$$j_{+\rho} F_{+\rho} = j_{-\rho} F_{-\rho}, \tag{28}$$

because $d_Q j_\rho = 0$. Using the definition of $\mathcal{A}_\rho$ and Eq. (28), we obtain:

$$e^{\mathcal{A}_\rho} = \frac{F_{-\rho}}{F_{+\rho}}. \tag{29}$$

At this point of optimal current, Eq. (27) defines a linear system of the form $\mathbb{M} \cdot \mathbf{F}_+ = 0$, because the elements of $\mathbf{F}_-$ can be expressed in terms of those of $\mathbf{F}_+$ by using the local affinities. The solutions of this system will be trivial if $\mathbb{M}$, which contains information on both the topology and the affinities, is not singular. Enforcing that the determinant of this matrix is zero results in a constraint involving solely the values of the optimal affinities and the elements of the stoichiometric matrices (see Supplementary Note 5). It does not require an explicit evaluation of the steady-state rates or concentrations, nor does it involve kinetic parameters. We illustrate this approach in the next section.

The condition on the determinant is useful, but cannot easily be applied to large CRNs. However, using Eq. (29), the affinity of the overall reaction can be expressed only in terms of the $F_{\pm\rho}$ at the optimal flux:

$$\mathcal{A}^* = \sum_\rho g_X^\rho \ln\left(\frac{F_{-\rho}}{F_{+\rho}} \right). \tag{30}$$

Finding a bound (a minimum or a maximum) for this global affinity corresponds to solving an optimization problem with Eq. (27) acting as linear constraints and additional constraints due to tight coupling and the second law as detailed in the Methods section below (see Eq. (39)). More details are provided in the Supplementary Note 11, where we establish conditions under which this optimization problem becomes concave. The solution to this optimization problem provides the thermodynamic bounds as well as information on the response coefficients using only the topology of the reaction network. As was the case with the method based on determinants, this link does not rely on an explicit evaluation of the steady-state fluxes or concentrations, nor does it require knowledge of kinetic parameters. In addition to this, the optimization approach can easily be used with large CRNs.

Since the bounds on the optimal affinity do not depend explicitly on the expressions of the steady-state concentrations or reaction rates, our method is applicable to large and complex networks, in which these concentrations and rates are too complex to be computed. For the same reason, the bounds hold even if the system features multistability, which is often found in autocatalytic networks[1]. We show this explicitly for the bistable Schlögl model[34] in Supplementary Note 15.

As an illustration of our approach, we derive lower bounds satisfied by the global affinity of the Hinshelwood autocatalytic cycle[35] with intermediate species, as represented in Fig. 3a. When the intermediate species, B or D, are controlled, the constraints on the $F_{\pm\rho}$s can be satisfied and the global flux has a zero-derivative maximum (see the blue curve in Fig. 3b). In that case, the affinity at the optimum of the current is lower-bounded,

$$\mathcal{A}^* \geq \ln 4, \tag{31}$$

and the bound can be approached as closely as desired with an appropriate choice of rate constants, as shown in Fig. 3c (blue triangles). When, instead, the concentration of A or C is maintained constant, the constraints acting on the $F_{\pm\rho}$s cannot be satisfied (see Supplementary Note 14). As a consequence, the global flux, $\mathcal{J}$, has no zero-derivative maximum and, then, is a decreasing function of Q whose largest value occurs at $Q = 0$ (see red curve in Fig. 3b), where the definition of the $F_{\pm\rho}$s and Eq. (28) do not apply. As a result, $\exp(\mathcal{A}^*)$ diverges. In addition to the Hinshelwood cycle, we also analyzed in Supplementary Note 13 all the autocatalytic cores[21]; the results are summarized in Table 1. Importantly, the bound found for the five autocatalytic cores remains valid if unimolecular segments of reactions are added to any of these networks (see Supplementary Note 10 and Supplementary Fig. 1).

Bounds for type I and type II networks

Now, two situations arise depending on whether species X appears or not as a reactant in the overall reaction. When species X is a reactant in the overall equation, the reaction vector $\mathbf{g}_X$ defines a seed-dependent mode of production[23,24]. In that case, the overall reaction is

$$\alpha X + (\diamond) \longrightarrow \beta X + (\diamond), \tag{32}$$
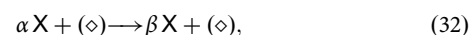
with α and β being integers such that $\beta > \alpha > 0$, and $(\diamond)$ represents all the spectator species. Note that in our formalism, the concentrations of the external species are absorbed in the rate constants, so these species do not appear explicitly in the overall reaction. The simplest network obeying Eq. (32) is a generalized version of the Type I core presented in example (1) with an arbitrary number of intermediate species. As shown in Supplementary
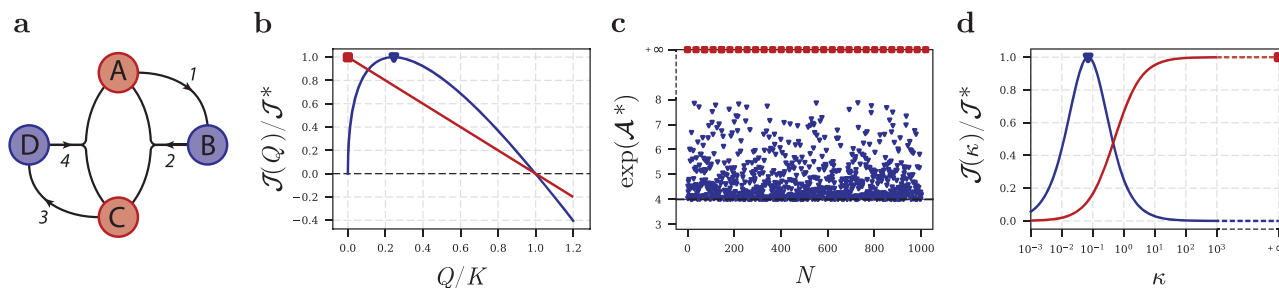
Fig. 3 | Optimal properties of the Hinshelwood cycle. a Schematic representation of the Hinshelwood cycle with two types of species: red species (A or C) and blue species (B or D). **b** Global flux normalized by its maximum value $\mathcal{J}^*$ as a function of Q/K when a specific species of the cycle is chemostatted. This flux has a zero-derivative maximum (blue triangle) if a blue species is chemostatted or simply reaches its maximal value at $Q = 0$ (red square) if a red species is chemostatted. **c** Cloud of points for the exponential of the global affinity $\mathcal{A}^*$, for randomly chosen sets of kinetic rate constants indexed by N. If a blue species is chemostatted, points are lower-bounded by 4 (blue triangles) otherwise, the affinity diverges (red squares). **d** Global flux normalized by its maximum value $\mathcal{J}^*$ as a function of the degradation rate κ of a specific species. When a blue species is degraded, a zero-derivative maximum exists and is reached at a finite value of κ, while if a red species is degraded, the global flux is monotonously increasing and reaches its maximal value at infinity. Simulation parameters for **b** and **d** are $k_{+1} = k_{+3} = 1$ and $k_{+2} = k_{+4} = k_{-1} = k_{-2} = k_{-3} = k_{-4} = 0.1$.

Note 8, the global production rate in a generalized Type I attains its maximum when

$$\mathcal{A}^* = \ln\left(\frac{\beta}{\alpha}\right). \tag{33}$$

Let us now consider a specific class of networks that we call non-intersecting, for which the stoichiometric matrix of the products, $\mathbb{S}_-$, is lower triangular up to permutations of species and reactions (see Supplementary Note 6). This means that in non-intersecting networks, each reaction only produces downstream species. We have shown that for non-intersecting networks, Eq. (33) represents the lowest achievable bound for $\mathcal{A}^*$ when the overall reaction is seed-dependent. We conjecture that this proposition is not restricted to non-intersecting networks but may hold in general.

Conversely, when species X is not present as a reactant in the overall reaction, the reaction vector $\mathbf{g}_X$ defines a seed-independent mode of production. In that case, the overall reaction reads

$$(\diamond) \longrightarrow \beta X + (\diamond), \tag{34}$$

where β is a strictly positive integer. It should be noted that Eq. (34) can describe overall reactions that are not necessarily derived from an autocatalytic network. However, the presence of an optimal flux and the bounds on the corresponding affinity can only be guaranteed if there is an underlying autocatalytic network present. The simplest topology compatible with Eq. (34) is a generalization of the Type II core:

$$\alpha X \rightleftarrows Y_1 \rightleftarrows \cdots \rightleftarrows Y_n \rightleftarrows Y_1 + \beta X. \tag{35}$$
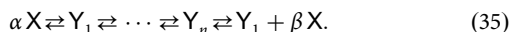
This network is also non-intersecting (see Supplementary Note 9) and the global affinity associated with the maximum of $\mathcal{J}$ is

$$\mathcal{A}^* = \ln\left(\frac{\beta}{\alpha} + 1\right). \tag{36}$$

Discussion

We presented a theoretical framework that allows to derive constraints on the affinity and on the concentrations of autocatalysts, in the regime where all the fluxes in the network are tightly coupled and the rate of autocatalytic production is maximal. In this specific regime and assuming mass-action law, the constraints can be derived using only the knowledge of the topology of the underlying reaction network but do not require a knowledge of the kinetics. In this final section, we discuss the potential applications of our work, its relation to non-equilibrium thermodynamics, and potential extensions.

Besides the tight coupling condition, the core ingredient of our work is the presence of a maximum for the macroscopic flux with respect to a certain control parameter. For simplicity, we derived our results assuming this parameter was directly related to a fixed concentration of one autocatalytic species, Q. However, there exists flexibility in selecting this parameter, as long as the tight coupling property Eq. (21) is preserved. In particular, tuning the concentration of a single autocatalyst, may not be very practical experimentally. A more manageable control parameter could be, for instance, a selective degradation using specific enzymes. For that case, we have checked that the property of tight coupling of the reaction fluxes is indeed preserved (see Eq. (44) in the Methods section). The macroscopic flux, $\mathcal{J}$, becomes now a function of a degradation rate constant κ and becomes zero for $\kappa = 0$ at equilibrium, and above a critical value κ_c (provided $\kappa_c < \infty$), where degradation overcomes the production of the X species by the autocatalytic network (see Eq. (45) in the Methods section). This threshold κ_c is experimentally accessible and has been considered before as a possible measure of fitness for autocatalytic networks[8]. Importantly, because the constraints on the $F_{\pm\rho}$ and the steady-state are unaffected by the control procedure (chemostat or degradation), the bounds remain unchanged if one considers a degradation instead of chemostat. We illustrated this point with the Hinshelwood cycle in Fig. 3d: when B or C are being degraded, the current has a zero-derivative maximum verifying $\mathcal{A}^* \geq \ln 4$. While, on the contrary, when A or D undergoes degradation, the current has no zero-derivative maximum and the overall affinity diverges.

The various bounds that we have encountered in this work measure how far from equilibrium a given network should be in order to deliver a maximal flux of autocatalytic production. It is advantageous for a given network to operate close to this point not only because the global reaction is fast, but also because the system is then robust: at this point, variations in the concentration of the autocatalytic species are buffered and hardly affect the flux, which is thus stable.

The affinity can also be interpreted as the entropy production associated with a steady production of species X[28] or, equivalently, as the production of entropy per autocatalytic cycle[8]. The bounds for the optimal affinities can thus be seen as the minimal cost required to maintain an optimal rate of autocatalytic production. We also observed that this minimal cost increases dramatically when certain reactions within the network are at equilibrium or when certain key species are depleted, as we have illustrated in the case of the Hinshelwood cycle. This is consistent with the idea that the thermodynamic cost should increase in a pathway when certain steps are at equilibrium[36,37].

Another natural extension of the present work would be to further investigate the thermodynamics of autocatalytic networks. It would be interesting to explore possible connections between this work and a number of studies on thermodynamic trade-offs between dissipation, speed, and accuracy, and other recent studies on the response of non-equilibrium Markovian systems to perturbations[38–40].

In this work, we were mainly interested in chemical networks in a well-mixed environment assuming mass-action kinetics. These assumptions are valid for elementary reactions in well-mixed and dilute solutions, but might prove unrealistic in crowded environments and/or where chemical species interact, such as in biological cells. Alternative kinetic laws, like Michaelis–Menten kinetics, could be used in our framework as long as there is an elementary level at which the law of mass-action holds, and the coarse-graining from that microscopic level only involves unimolecular reactions. Thus, the assumption of mass-action law is an important limitation of our work, but it is the price to pay to obtain bounds which are independent of the kinetics. Similarly, a recent work reported a method to compute concentration ranges for metabolites in the absence of knowledge from kinetics but the method is only applicable for mass-action law networks in the limit of dilute systems[20].

Our framework could be used as a computational approach to predict concentration ranges and thermodynamic affinities from large-scale metabolic models, which could be useful for the design of autocatalytic or self-replicating systems[36]. It could also be used to provide information on the topological complexity of observed chemical networks. Indeed, we observed that the bounds tend to increase with the topological complexity of the network, as shown in Table 1. One measure of topological complexity is the connectivity of the network, and precisely, we have shown that the bound increases with the degree of branching of a reaction when the network contains only one such reaction (see Supplementary Note 7). A generalization beyond this case may be within reach.

Finally, we note that autocatalytic systems are of particular importance for scenarios on the origin of life. Autocatalytic networks can amplify initially small numbers of molecules and the rate at which such species are produced would certainly play a role in the competition between molecules. In this context, running at an optimal and robust production rate could provide an autocatalytic network with a significant advantage in terms of chemical selection. It would thus be interesting to further explore the consequences of this framework for assessing the robustness and the evolvability of autocatalytic networks.

Methods
Setup and notation
We assume that the chemical reaction network (CRN) is described by a stoichiometric matrix of the form

$$
\nabla = \mathcal{E} \left\uparrow \begin{pmatrix} \nabla^{\mathrm{ex}} \\ \cdots \cdots \cdots \\ \mathbb{S} \vdots \mathbf{0} \\ \vdots \end{pmatrix} \right.,
$$
$$
\underset{\mathcal{P}}{\longleftarrow}
$$
(37)

where $\mathcal{E}$ is the set of all species and $\mathcal{P}$ is the set of all reactions in the full system. The restriction of ∇ on $\mathcal{E}^{\mathrm{ex}}$ (denoted ∇^{ex}) describes external species, while $\mathbb{S}$ is the stoichiometric matrix of autocatalytic species. By assumption, it is a square invertible matrix. Thus, one has $\mathcal{E} = \mathcal{E}^{\mathrm{ex}} \cup \mathcal{Z}$ and $\mathcal{P} = \mathcal{P}^{\mathrm{ex}} \cup \mathcal{R}$, where $\mathcal{Z}$ is the set of autocatalytic species and $\mathcal{R}$ is the set of autocatalytic reactions. The autocatalytic network is coupled to external species in $\mathcal{E}^{\mathrm{ex}}$ which are involved in additional reactions $\mathcal{P}^{\mathrm{ex}}$. Note that a somewhat similar matrix decomposition has already been introduced to study the geometrical features of non-equilibrium reaction networks[12].

After chemostatting all the external species, the autocatalytic CRN is still able to reach detailed balance. To see this, one can multiply the matrix ∇ on its left-hand side by the row vector $(\boldsymbol{\mu}_{\mathrm{ex}}, \boldsymbol{\mu})$ where $\boldsymbol{\mu}_{\mathrm{ex}}$ are the chemical potentials of the external species and $\boldsymbol{\mu}$ the chemical potentials of the autocatalytic species. This yields $\boldsymbol{\mu}_{\mathrm{ex}} \cdot (\nabla^{\mathrm{ex}})_{\mathcal{R}} + \boldsymbol{\mu} \cdot \mathbb{S}$, with $(\nabla^{\mathrm{ex}})_{\mathcal{R}}$ being the restriction of ∇^{ex} to the space of autocatalytic reactions $\mathcal{R}$. As $\mathbb{S}$ is non-singular, a solution that satisfies detailed balance always exists:

$$
\boldsymbol{\mu}^{\mathrm{eq}} = -\boldsymbol{\mu}_{\mathrm{ex}} \cdot (\nabla^{\mathrm{ex}})_{\mathcal{R}} \cdot \mathbb{S}^{-1}.
$$
(38)

This means that the autocatalyic CRN is able to reach an equilibrium state even though the additional reactions $\mathcal{P}^{\mathrm{ex}}$ are kept away from equilibrium ($\boldsymbol{\mu}_{\mathrm{ex}} \cdot (\nabla^{\mathrm{ex}})_{\mathcal{P}^{\mathrm{ex}}} \neq \mathbf{0}$).

Additional constraints
Applying the second law of thermodynamics on Eq. (25) imposes that the global flux is positive for $Q \in [0, K[$ and negative for $Q \geq K$ thus, Q^* lies in $[0, K[$, where $\mathcal{J}(Q^*) > 0$. Then, because of the tight coupling condition Eq. (21), the signs of j_ρ and g_X^ρ are the same. Further, if $g_X^\rho > 0$ then $j_\rho > 0$ and thus $\mathcal{A}_\rho > 0$; conversely, if $g_X^\rho < 0$ then $j_\rho < 0$, yielding $\mathcal{A}_\rho < 0$. We are then left with the special and important case where $g_X^\rho = 0$, which implies that both j_ρ and $\mathcal{A}_\rho = 0$ vanish. In that case, the corresponding reaction ρ is at equilibrium. To summarize :

$$
\forall \rho \in \mathcal{R}, \, g_X^\rho \mathcal{A}_\rho > 0, \quad \text{and} \quad \mathcal{A}_\rho = 0 \quad \text{when} \quad g_X^\rho = 0.
$$
(39)

Note that these conditions directly translate into additional non-linear constraints on the $F_{\pm\rho}$s at the optimum.

Rescaled modes of production
Because $\mathbb{S}$ is integer-valued, there exists a smallest $n \in \mathbb{N}^*$ such that $n \mathbb{S}^{-1}$ is also integer-valued. The columns of $n \mathbb{S}^{-1}$ define the rescaled modes of production. From Eq. (24), along these rescaled modes, the global affinity is $n \mathcal{A}$. Since the value of each of the elementary fluxes needs to remain unchanged, the tight coupling condition Eq. (21) implies that the macroscopic current should be $\mathcal{J}/n$ after the rescaling. As a result, from Eq. (25), the EPR is preserved by the rescaling. In Eqs. (32) and (34), we implicitly used the rescaled modes of production so that $\alpha, \beta \in \mathbb{N}$.

Extension to the case of specific degradation
We show here that the bounds derived by considering that an autocatalytic species is chemostatted remain valid when the chemostatting procedure is replaced by a specific degradation of the same species. Let us call X the autocatalytic species in question. We can introduce an augmented stoichiometric matrix and an augmented flux vector to take into account the degradation:

$$
\mathbb{S}' = \begin{pmatrix} \mathbf{S}^X & \vdots & -1 \\ \vdots & & \vdots \\ \mathbb{S}^Y & \vdots & \mathbf{0} \end{pmatrix}, \qquad \mathbf{v} = \begin{pmatrix} \mathbf{j} \\ \kappa \, f(x) \end{pmatrix},
$$
(40)

where κ is non-negative. The degradation rate is described by the function $f(x)$, which can be a simple power law x^n with $n > 0$, or a more sophisticated expression, such as a Hill function:

$$
f(x) = \frac{x^n}{x^n + K},
$$
(41)

in which K is usually referred to as the apparent dissociation constant. The Hill function is often used to model kinetics involving the fixation of a substrate on macromolecules (such as proteins), and includes the Michaelis–Menten law as a special case (i.e., $n = 1$). The dynamics of such an extended system obeys

$$
\mathrm{d}_t \mathbf{z} = \mathbb{S}' \cdot \mathbf{v}.
$$
(42)

A steady state of this new system consists of $\mathbf{v} \in \ker[\mathbb{S}']$, the latter being spanned by $\mathbf{g}'_X = (\mathbf{g}_X, 1)^\top$,

$$
\mathbb{S}' \cdot \mathbf{g}'_X = \begin{pmatrix} \mathbf{S}^X \cdot \mathbf{g}_X - 1 \\ \mathbb{S}^Y \cdot \mathbf{g}_X \end{pmatrix} = \mathbf{0}.
$$
(43)

Consequently, the steady elementary fluxes associated with Eq. (42) are proportional to $\mathbf{g}'_X$, implying the tight-coupling condition:

$$\mathbf{j} = \mathcal{J}(\kappa)\,\mathbf{g}_X. \tag{44}$$

The steady-state fluxes of the various reactions still follow the law of mass action Eq. (23), but are now parameterized by κ instead of Q. Consequently, we recover the definition of the $F_{\pm\rho}$s as the log-derivatives of the elementary fluxes Eq. (26). From that, the structural constraints Eq. (27) follow.

At steady-state, the tight coupling condition Eq. (44) implies:

$$\mathcal{J}(\kappa) = \kappa f(x). \tag{45}$$

Hence, the global flux necessarily vanishes when $\kappa = 0$ because the system reaches equilibrium in the absence of degradation. Additionally, Eq. (45) implies that $\mathcal{J}(\kappa) \geq 0$, which allows us to recover the additional constraints derived above. We now introduce $\kappa_c \in\ ]0, +\infty]$, which is defined as the value of the degradation rate such that $x(\kappa_c) = 0$. If $\kappa_c < +\infty$ then, for any $\kappa \geq \kappa_c$, $x(\kappa) = 0$ is the only physically acceptable solution, so that Eq. (45) implies $\mathcal{J}(\kappa) = 0$ as well. On the other hand, if κ_c diverges, Eq. (45) imposes that

$$x(\kappa)^n \underset{+\infty}{\sim} \kappa^{-\alpha}, \ \alpha \geq 1. \tag{46}$$

From that, two qualitatively different situations can be found. If $\alpha > 1$, the global flux tends to vanish as κ goes to infinity: $\mathcal{J}(+\infty) = 0$. Instead, if $\alpha = 1$, the global flux converges to a finite non-zero value, $\mathcal{J}(+\infty) > 0$. Such systems are similar to those having a non-vanishing global flux when $Q = 0$ in the chemostatted case. As before, if the constraints are incompatible, $\mathcal{J}(\kappa)$ is a monotonous function, attaining its maximum when the X species is completely depleted, as shown by the red curve in Fig. 3d. In the system with specific degradation, this corresponds to impose a diverging degradation rate, $\kappa^* = \kappa_c = +\infty$.

Data availability
The data points used in the Figs. 1 and 3 are available from the corresponding author upon request.

Code availability
The code that generated the plots is available from the corresponding author upon reasonable request.

References
1. Schuster, P. What is special about autocatalysis? *Monatsh. Chemie* **150**, 763 (2019).
2. Xavier, J. C., Hordijk, W., Kauffman, S., Steel, M. & Martin, W. F. Autocatalytic chemical networks at the origin of metabolism. *Proc. R. Soc. B Biol. Sci.* **287**, 20192377 (2020).
3. Lin, W. H., Kussell, E., Young, L. S. & Jacobs-Wagner, C. Origin of exponential growth in nonlinear reaction networks. *Proc. Natl Acad. Sci. USA* **117**, 27795 (2020).
4. Roy, A., Goberman, D. & Pugatch, R. A unifying autocatalytic network-based framework for bacterial growth laws. *Proc. Natl Acad. Sci. USA* **118**, e2107829118 (2021).
5. Ameta, S., Matsubara, Y. J., Chakraborty, N., Krishna, S. & Thutupalli, S. Self-reproduction and darwinian evolution in autocatalytic chemical reaction systems. *Life* **11**, 308 (2021).
6. Lancet, D., Zidovetzki, R. & Markovitch, O. Systems protobiology: origin of life in lipid catalytic networks. *J. R. Soc. Interface* **15**, 20180159 (2018).
7. Schrödinger, E. *What is Life? The Physical Aspect of the Living Cell* (Cambridge Univ. Press, 1944).
8. Kolchinsky, A. A thermodynamic threshold for darwinian evolution. Preprint at arXiv https://doi.org/10.48550/arXiv.2112.02809 (2021).
9. Pascal, R., Pross, A. & Sutherland, J. D. Towards an evolutionary theory of the origin of life based on kinetics and thermodynamics. *Open Biol.* **3**, 130156 (2013).
10. Endres, R. G. Entropy production selects nonequilibrium states in multistable systems. *Sci. Rep.* **7**, 1 (2017).
11. George, A. B., Wang, T. & Maslov, S. Functional convergence in slow-growing microbial communities arises from thermodynamic constraints. *ISME J.* **17**, 1482 (2023).
12. Dal Cengio, S., Lecomte, V. & Polettini, M. Geometry of nonequilibrium reaction networks. *Phys. Rev. X* **13**, 021040 (2023).
13. Avanzini, F., Penocchio, E., Falasco, G. & Esposito, M. Nonequilibrium thermodynamics of non-ideal chemical reaction networks. *J. Chem. Phys.* **154**, 94114 (2021).
14. Hirono, Y., Okada, T., Miyazaki, H. & Hidaka, Y. Structural reduction of chemical reaction networks based on topology. *Phys. Rev. Res.* **3**, 043123 (2021).
15. Sughiyama, Y., Loutchko, D., Kamimura, A. & Kobayashi, T. J. Hessian geometric structure of chemical thermodynamic systems with stoichiometric constraints. *Phys. Rev. Res.* **4**, 033065 (2022).
16. Yoshimura, K. & Ito, S. Information geometric inequalities of chemical thermodynamics. *Phys. Rev. Res.* **3**, 013175 (2021).
17. Orth, J. D., Thiele, I. & Palsson, B. O. What is flux balance analysis? *Nat. Biotechnol.* **28**, 245 (2010).
18. Fell, D. & Cornish-Bowden, A. *Understanding the Control of Metabolism* Vol. 2 (Portland Press, 1997).
19. Steuer, R., Gross, T., Selbig, J. & Blasius, B. Structural kinetic modeling of metabolic networks. *Proc. Natl Acad. Sci. USA* **103**, 11868 (2006).
20. Küken, A., Eloundou-Mbebi, J. M. O., Basler, G. & Nikoloski, Z. Cellular determinants of metabolite concentration ranges. *PLoS Comput. Biol.* **15**, 1 (2019).
21. Blokhuis, A., Lacoste, D. & Nghe, P. Universal motifs and the diversity of autocatalytic systems. *Proc. Natl Acad. Sci. USA* **117**, 25230 (2020).
22. Unterberger, J. & Nghe, P. Stoechiometric and dynamical autocatalysis for diluted chemical reaction networks. *J. Math. Biol.* **85**, 26 (2022).
23. Andersen, J. L., Flamm, C., Merkle, D. & Stadler, P. F. Defining autocatalysis in chemical reaction networks. Preprint at https://doi.org/10.48550/arXiv.2107.03086 (2021).
24. Peng, Z., Linderoth, J. & Baum, D. A. The hierarchical organization of autocatalytic reaction networks and its relevance to the origin of life. *PLoS Comput. Biol.* **18**, 1 (2022).
25. Arya, A. et al. An open source computational workflow for the discovery of autocatalytic networks in abiotic reactions. *Chem. Sci.* **13**, 4838 (2022).
26. Wachtel, A., Rao, R. & Esposito, M. Thermodynamically consistent coarse graining of biocatalysts beyond Michaelis-Menten. *N. J. Phys.* **20**, 042002 (2018).
27. Rao, R. & Esposito, M. Nonequilibrium thermodynamics of chemical reaction networks: wisdom from stochastic thermodynamics. *Phys. Rev. X* **6**, 041064 (2016).
28. Polettini, M. & Esposito, M. Irreversible thermodynamics of open chemical networks. I. Emergent cycles and broken conservation laws. *J. Chem. Phys.* **141**, 024117 (2014).
29. Qian, H. & Beard, D. A. Thermodynamics of stoichiometric biochemical networks in living systems far from equilibrium. *Biophys. Chem.* **114**, 213 (2005).
30. Feinberg, M. *Foundations of Chemical Reaction Network Theory* (Springer, 2019).
31. Pekar^, M. *Progress in Reaction Kinetics and Mechanism* Vol. 30 (Science Reviews Ltd, 2005).

32. Kondepudi, D. & Prigogine, I. *Modern Thermodynamics* (John Wiley & Sons, Ltd, 2014).
33. Baiesi, M. & Maes, C. Life efficiency does not always increase with the dissipation rate. *J. Phys. Commun.* **2**, 45017 (2018).
34. Vellela, M. & Qian, H. Stochastic dynamics and non-equilibrium thermodynamics of a bistable chemical system: the Schlögl model revisited. *J. R. Soc. Interface* **6**, 925 (2009).
35. Hinshelwood, C. N. On the chemical kinetics of autosynthetic systems. *J. Chem. Soc*. 745–755 (1952).
36. Barenholz, U. et al. Design principles of autocatalytic cycles constrain enzyme kinetics and force low substrate saturation at flux branch points. *eLife* **6**, e20667 (2017).
37. Noor, E. et al. Pathway thermodynamics highlights kinetic obstacles in central metabolism. *PLoS Comput. Biol.* **10**, e1003483 (2014).
38. Owen, J. A. & Horowitz, J. M. Size limits the sensitivity of kinetic schemes. *Nat. Commun.* **14**, 1280 (2023).
39. Liang, S., Rios, P. D. L. & Busiello, D. M. Thermodynamic bounds on symmetry breaking in biochemical systems. *Phys. Rev. Lett.* **132**, 2284022024 (2024)
40. Aslyamov, T. & Esposito, M. Nonequilibrium response for Markov jump processes: exact results and tight bounds. *Phys. Rev. Lett.* **132**, 037101 (2024).

Author contributions
Y.D.D. and D.L. designed the research and received funding. A.D. performed the research. A.D., Y.D.D., and D.L. wrote the paper.

Competing interests
The authors declare no competing interests.

Additional information
Supplementary information The online version contains supplementary material available at https://doi.org/10.1038/s42005-024-01704-8.

Correspondence and requests for materials should be addressed to Armand Despons.

Peer review information *Communications Physics* thanks the anonymous reviewers for their contribution to the peer review of this work.

Reprints and permissions information is available at http://www.nature.com/reprints

Publisher's note Springer Nature remains neutral with regard to jurisdictional claims in published maps and institutional affiliations.